

# Computational Fluid Dynamics Evaluation of Equivalency in Hemodynamic Alterations Between Driver, Integrity, and Similar Stents Implanted Into an Idealized Coronary Artery

**Timothy J. Gundert**

Department of Biomedical Engineering,  
Marquette University,  
1515 West Wisconsin Avenue,  
Milwaukee, WI 53233

**Ronak J. Dholakia**

Department of Neurological Surgery,  
Stony Brook University Medical Center,  
Stony Brook, NY 11794

**Dennis McMahon**

Medtronic CardioVascular,  
3576 Unocal Place,  
Santa Rosa, CA 95403

**John F. LaDisa, Jr.<sup>1</sup>**

Department of Biomedical Engineering,  
Marquette University,  
1515 West Wisconsin Avenue,  
Milwaukee, WI 53233;  
Department of Medicine,  
Division of Cardiovascular Medicine,  
Medical College of Wisconsin,  
8701 Watertown Plank Road,  
Milwaukee, WI 53226  
e-mail: john.ladisa@marquette.edu

*We tested the hypothesis that a slight modification in fabrication from the Driver to the Integrity stent (Medtronic) results in nearly equivalent distributions of wall shear stress (WSS) and mean exposure time (MET), reflective of flow stagnation, and that these differences are considerably less than the Multi-Link Vision (Abbott Vascular) or BX Velocity (Cordis) bare metal stents when evaluated by computational fluid dynamics (CFD). Arteries were modeled as idealized straight rigid vessels without lesions. Two vessel diameters (2.25 and 3.0 mm) were studied for each stent and 2.75 mm diameter Integrity stents were also modeled to quantify the impact from best- and worst-case orientations of the stent struts relative to the primary blood flow direction. All stents were 18 mm in length and over-deployed by 10%. The results indicated that, regardless of diameter, the BX Velocity stents had the greatest percentage of the vessel exposed to adverse WSS followed by the Vision, Integrity, and Driver stents. In general, when strut thickness and stent:lumen ratio are similar, the orientation of struts is a determining factor for deleterious flow patterns. For a given stent, the number of struts was a larger determinant of adverse WSS and MET than strut orientation, suggesting that favorable blood flow patterns can be achieved by limiting struts to those providing adequate scaffolding. In conclusion, the Driver and Integrity stents both limit their number of linkages to those which provide adequate scaffolding while also maintaining similar strut thickness and stent:lumen ratios. The Integrity stent also imparts a slight helical velocity component. The modest difference in the fabrication approach between the Driver and Integrity stents is, therefore, not hemodynamically substantial in this idealized analysis, particularly relative to potentially adverse flow conditions introduced by the other stents modeled. This data was used in conjunction with associated regulatory filings and submitted to the FDA as part of the documents facilitating the recent approval for sale of the Resolute Integrity stent in the United States. [DOI: 10.1115/1.4023413]*

## Introduction

Previous computational and experimental studies have shown an association between alterations in local blood flow patterns established after coronary stenting and sites of increased neointimal hyperplasia (NH), which is the primary component of restenosis [1,2]. Additionally, stagnation zones have been shown to correlate with regions at higher risk of stent thrombosis [3]. Clinical studies have demonstrated that restenosis rates and other important endpoints are dependent upon the geometric properties of the implanted coronary stent, including such details as stent strut thickness [4–6]. Collectively, these prior findings indicate that the local blood flow environment created by the implantation of a coronary stent can uniquely influence the local neointimal response, thrombotic potential, and clinical sequelae.

Medtronic created the Integrity coronary stent through a modification to their predicate device, the Driver stent. The Driver stent is created from single rings of cobalt alloy. Each ring is formed

into a sinusoidal segment. The individual segments are then laser fused at specific crowns to produce the overall geometric pattern (see Fig. 1). The Integrity stent is formed from a single wire of the same cobalt alloy as the Driver stent. In creating the Integrity stent, the cobalt alloy wire is formed into a repeating sinusoidal pattern of crowns and struts which are then wound around a mandrel. Understanding the clinical issues surrounding changes in stent geometries, Medtronic minimized changes to any factor that had the potential to impact the stent geometry. The radial strength, strut size and shape, and stent metal remained unchanged between devices.

The current investigation was, therefore, conducted to test the hypothesis that this manufacturing change was not hemodynamically substantial. Since the Integrity stent has been designed to have similar strut geometries and deployed cross-sectional area as the predicate Driver stent, the potential for NH and thrombogenicity from a hemodynamic perspective are expected to be similar; therefore, limiting the likelihood of adverse safety and efficacy from related indices. Specifically, the slight modification in fabrication methods from the Driver stent to the Integrity stent was hypothesized to display nearly equivalent distributions of wall shear stress (WSS) and flow stagnation patterns between the two

<sup>1</sup>Corresponding author.

Manuscript received July 24, 2012; final manuscript received January 2, 2013; published online February 4, 2013. Assoc. Editor: Keefe B. Manning.

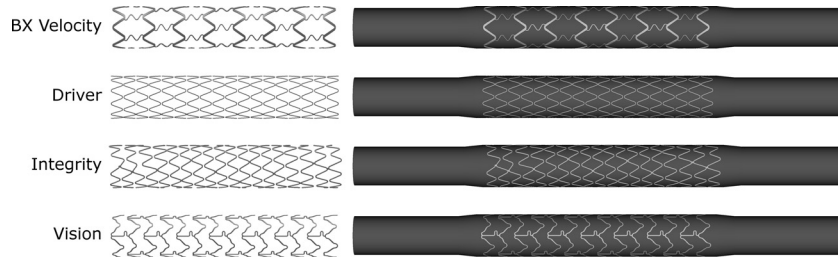


**Fig. 1 Computer-aided design representations of the Integrity (Medtronic), Driver (Medtronic), Multi-Link Vision (Abbott Vascular), and BX Velocity (Cordis) stents before (left) with stents longitudinally sectioned for clarity, and after virtual implantation into an idealized artery using 10% over-deployment (right)**

**Table 1 Commercially-available stents for CFD analysis**

Stent	Manufacturer	Sizes
Integrity	Medtronic	$2.25 \times 18$ ; $2.75 \times 18$ ; $3.0 \times 18$
Driver	Medtronic	$2.25 \times 18$ and $3.0 \times 18$
Multi-Link Vision	Abbott Vascular	$2.25 \times 18$ and $3.0 \times 18$
BX Velocity	Cordis	$2.25 \times 18$ and $3.0 \times 18$

stents, rendering the data useful to accompany the associated pre-market application FDA submission for the Resolute Integrity and the Integrity Shonin submission in Japan. It was further hypothesized that the difference between the Driver and the Integrity stent would be considerably less than between other commercially available bare metal stents when evaluated using computational fluid dynamics (CFD) modeling.

## Methods

**Creation of CFD Models.** Arteries were modeled as idealized straight and rigid vessels without lesions to isolate local disturbances caused by geometric stent features and for comparison to previous work [7–9]. Bare metal coronary stents mimicking geometric features of the Integrity (Medtronic), Driver (Medtronic), Multi-Link (ML) Vision (Abbott Vascular), and BX Velocity (Cordis) devices were created using computer-aided design software [10]. Two vessel diameters (2.25 and 3.0 mm) were studied for each stent (see Fig. 1 and Table 1). Two additional versions of a 2.75 mm diameter Integrity stent were modeled to quantify differences in the indices of interest from the best- and worst-case alignment of struts with respect to the primary blood flow direction within a given crown configuration. For example, the 2.75 mm Integrity stent modeled with 7.5 crowns has a greater angle of intersection relative to the primary direction of fluid flow when compared to the same crown configuration placed in a 2.25 mm vessel. However, the stent-to-vessel ratio will be greater for the 2.25 mm diameter version. Similarly, a 2.75 mm diameter Integrity stent modeled with 9.5 crowns will have a greater percentage of the vessel in contact with stent struts, but the angle of intersection of these struts, with respect to the primary direction of fluid flow, will be less. All stents were 18 mm in length, which is a commonly implanted coronary stent length, in order to compare differences among stent designs. Stent geometry information was obtained from the available manufacturer's product literature and physical measurements (see Table 2). A 10% over-deployment of the stent was implemented, consistent with prior studies and clinical guidelines [5,9]. Stents were assumed to have half of their thickness embedded into the vessel wall, as has been noted after stent deployment in optical coherence tomography (OCT) studies [11]. The vessel was assumed to expand circularly and not have differential expansion between stent struts, thereby minimizing the allowed protrusion of the vessel between struts.

**Computational Simulations.** Following model generation, the solid model of the implanted stent was discretized into a mesh of tetrahedral elements using MeshSim (Simmetrix, Clifton Park, NY). Initially, CFD models were discretized and adapted through successive simulations using MeshSim to create anisotropic meshes that reduced the computational cost as compared to isotropic meshes. While this approach allows for the determination of the optimal edge size within intrastrut regions, the adaption process uses velocity information [12,13] and, hence, provides less control over the number of elements in regions of low velocity within a stented region. Fortunately, MeshSim also allows a user to explicitly define edge lengths near a given CFD model face, such as struts or the vessel wall, through its interface within the Simvascular software package (simtk.org). Smooth transitions between differences in mesh density are then created between adjacent elements regardless of edge size. Thus, the optimal element size within the intrastrut regions was determined from adapted simulations and assigned near stent struts along with the vessel wall for the final simulation corresponding to each stent. A more coarse mesh was also prescribed in the proximal and distal unstented regions. Additional mesh refinement studies were not necessary once the intrastrut edge lengths were determined and applied to the final simulation since the total number of elements (2.25 mm diameter vessels = 2.6–3.0 million elements; 3.0 mm diameter vessels =  $3.0\text{--}3.8 \times 10^6$  elements) exceeded that used with the adapted meshes and the edge size was based on the minimum element dimensions from intrastrut regions (see Fig. 2). This approach is further supported by a recent optimization study in which increasing the number of elements beyond that provided here had no impact on a cost function rooted in WSS values extracted from intrastrut regions [8]. Briefly, an initial optimization was performed using mesh generation parameters that resulted in roughly 3–4 million element meshes for each model. A second optimization was then performed using parameters that created 6–8 million element meshes. The greatest difference in cost was <0.25% between models with an equal vessel diameter but different mesh density. Since doubling the mesh size only resulted in small variations in the computed cost and the optimal finding, the results were assumed to be independent of the computational mesh and the meshing parameters used to generate 3–4 million element meshes were used throughout the entire prior study and applied with the current investigation.

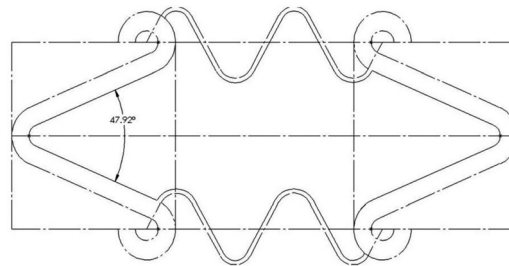
Computational arteries were assumed to be rigid and a no-slip boundary condition was prescribed on the vessel and stent surfaces. A left-anterior descending coronary artery flow waveform [14] with characteristics similar to those found in humans was imposed at the model inlet using a Womersley velocity profile [7–9,15–17]. Blood was assumed to be a Newtonian fluid with a density of  $1.06 \text{ g/cm}^3$  and a viscosity of 4 cP.

Outlet boundary conditions were prescribed using a three-element Windkessel approximation, consisting of characteristic ( $R_c$ ) and distal ( $R_d$ ) resistances, along with a capacitance ( $C$ ) term, in order to replicate the physiologic impedance of the downstream vasculature, as previously described [17–19].

**Table 2 Summary of stent design characteristics and legend demonstrating how the angle of struts relative to the primary flow direction was defined (below)**

Stent design	Vessel diameter (mm)	Stent diameter (mm)	Total area of stented region (mm <sup>2</sup> )	Lumen area (mm <sup>2</sup> )	Stent area (mm <sup>2</sup> )	Stent: lumen area	Area of repeating unit (mm <sup>2</sup> )	Number of subunits/ repeating unit	Area of subunit (mm <sup>2</sup> )	Angle relative to flow (deg)	Strut profile	Radial strut width/ diameter (mm)	Strut protrusion (mm; 50% embedded)
Integrity	2.250	2.475	140.0	115.7	24.3	0.21	4.866	4	1.217	42.1	Circular	0.0889	0.04445
	2.750	3.025	171.1	146.4	24.7	0.17	6.086	4	1.522	57.5	Circular	0.0889	0.04445
	2.750 <sup>a</sup>	3.025	171.1	139.6	31.5	0.23	3.013	5	0.603	48.2	Circular	0.0889	0.04445
	3.000	3.300	186.6	154.8	31.8	0.21	3.237	5	0.647	55.5	Circular	0.0889	0.04445
Driver	2.250	2.475	140.0	122.9	17.0	0.14	8.198	7	1.171	40.4	Circular	0.0889	0.04445
	3.000	3.300	186.6	161.9	24.7	0.15	4.460	5	0.892	43.8	Circular	0.0889	0.04445
BX Velocity	2.250	2.475	140.0	118.3	21.6	0.18	2.621	1	2.621	47.9	Rectangular	0.1397	0.06985
	3.000	3.300	186.6	160.6	26.1	0.16	3.489	1	3.489	72.7	Rectangular	0.1397	0.06985
ML Vision	2.250	2.475	140.0	118.1	21.8	0.18	2.836	1	2.836	75.2–84.3	Rectangular	0.08128	0.04064
	3.000	3.300	186.6	163.9	22.7	0.14	3.858	1	3.858	110.4–119.5	Rectangular	0.08128	0.04064

<sup>a</sup>Denotes undersized vessel.



Computational fluid dynamics simulations were run using an in-house stabilized finite element solver with a commercial linear solver component LESLIB (Altair Engineering, Troy, MI) to solve the time-dependent Navier–Stokes equations. The time step was chosen for a Courant, Friedrichs, and Lewy condition  $<1$ . Standard convergence criteria were employed and simulations were run until the outlet pressure and flow were periodic, defined as a maximum error between equivalent points in successive cardiac cycles  $<1$  mmHg and  $<1$  mm<sup>3</sup>/s (Fig. 3). The time-averaged

WSS (TAWSS) was then computed over the last cardiac cycle, as previously described [20]. This represented the third cardiac cycle for simulations conducted in the current study.

**Quantification of Results.** Indices of interest including velocity, MET, and distributions of WSS were quantified from converged simulation results. Flow stasis was quantified by computing the MET [21]. Using a particle tracking scheme with the converged CFD simulation results, the MET provides a measure of the average duration that particles reside within various regions of the model. Previous MET studies have released a uniform concentration of particles from the inlet of the model over the course of one cardiac cycle that were advected for several more cycles until all of the particles exited the domain. In this investigation, the inlet release strategy was not suitable for resolving the MET near stent struts because very few particles are released near the vessel wall due to low velocity in this region. Therefore, for the current study, a high concentration of particles was also released within 100  $\mu$ m of the stent struts and vessel wall at 25 time points throughout the cardiac cycle to better resolve the MET in these areas.

While time-varying changes in the WSS may have a clinical impact, the role of these temporal alterations in the mechano-transduction responsible for atherosclerosis or restenosis is not presently known in detail. Therefore, it is common to compute TAWSS over the cardiac cycle and evaluate the results relative to a threshold pertinent for a particular region of the vasculature [22]. All WSS results were normalized by the average TAWSS value in the proximal unstented region of each vessel. This step was necessary since the same inflow waveform was used for all models, regardless of vessel size.

In addition to the threshold method for comparing indices of the WSS, Murphy and Boyle recently discussed another way of displaying related indices within intrastrut regions [23]. The method provides a histogram of binned WSS values within

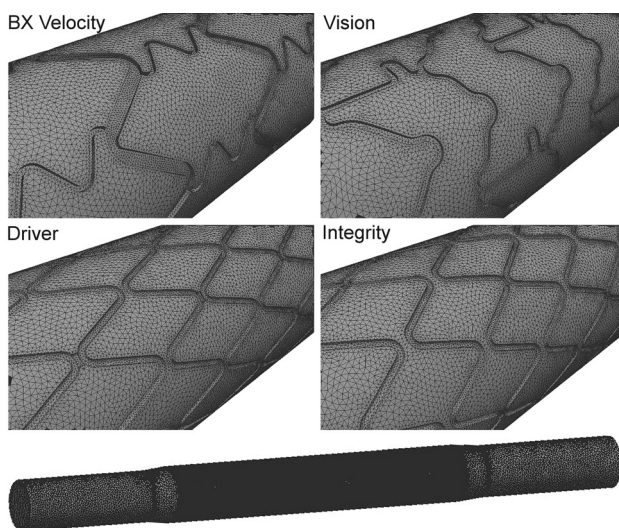


**Fig. 2 Final computational meshes used for each stent and a wide angle view showing increased mesh density within the stented region, as compared to the proximal and distal unstented regions**

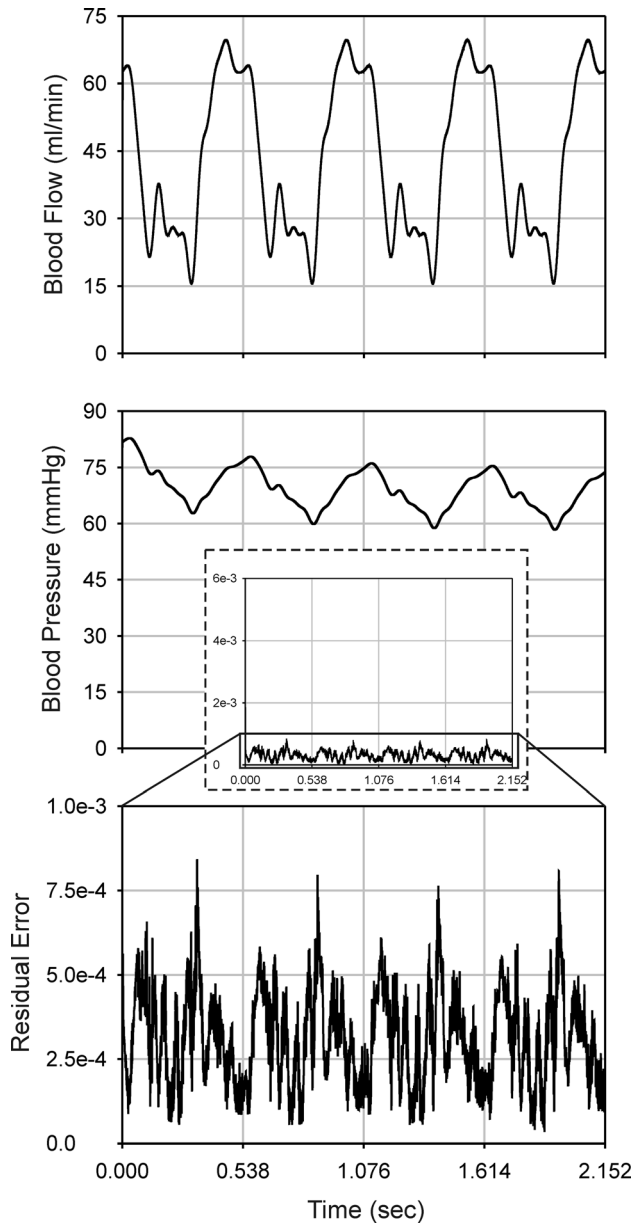


**Fig. 3** Blood flow at the outlet of the 3 mm diameter BX Velocity stent (top) and corresponding blood pressure (middle). Gridlines have been added to delineate each cardiac cycle and evolution of blood flow and pressure values between successive cardiac cycles. (inset) The residual error for the entire simulation is also shown along with that after the first four time steps (bottom). These tracings are similar for all of the stents modeled.

intrastrut regions that are normalized to the respective intrastrut area of each stent studied. This approach can help to more clearly appreciate any differences between stents.

The oscillatory shear index (OSI) was not quantified since only a modest portion (i.e.,  $\sim 1\%$ ) of the luminal surface was expected to be exposed to OSI ( $>0.1$ ) regardless of vessel diameter or the stent that was modeled in the current investigation. This outcome is anticipated given the straightness of the idealized vessels and characteristics of these stents with relatively thin struts. Although pronounced areas of elevated OSI would likely occur in the proximal vessel-to-stent transition region, flow disruption in this region would occur regardless of the implanted stent and be relatively modest when compared to TAWSS.

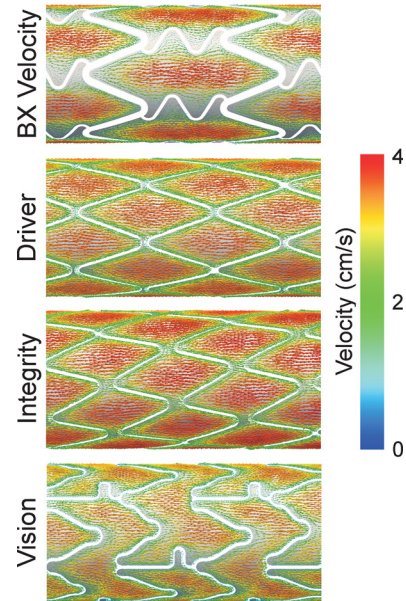


**Fig. 4** Magnitude-weighted near-wall velocity vectors (range: 0 to 4 cm/s) from the middle portions of each 2.25 mm diameter vessel. Vectors have been superimposed on the model surface and stent struts have been removed for clarity.

When the general behavior observed in 2.25 and 3.0 mm diameter vessels was similar, the diameter that more distinctively displayed this behavior was presented in the figure, depicting a particular index of interest for brevity and to limit the number and redundancy of figures.

## Results

### Comparison Between Different Commercially-Available Stents.

Near-wall velocity patterns within the proximal, distal, and middle portions of stents are provided in Fig. 4. The figure shows velocity vectors 0.05 mm from the wall during peak systole for all 2.25 mm diameter models. The size, color, and orientation of vectors highlight the flow patterns resulting from the implanted stent geometry. The local velocity is lowest in the proximal portion of all stents, but generally establishes a repeating pattern by the middle portion that was similar through the remaining distal sections of a given stent. The velocity was also low surrounding stent struts and particularly pronounced for the Vision stent, where the angle of intersection relative to the primary direction of fluid flow is greatest (see Table 2) and the number of longitudinally-oriented connector elements is fewest. Strut thickness is greatest for the BX Velocity stent and, although the vectors in Fig. 4 reveal low velocity near stent struts and connector elements, the speed of blood is still elevated and similar to the Integrity and Driver stents within the middle of intrastrut regions. Velocity patterns were similar for the Integrity and Driver stents. There were fewer areas of low velocity relative to the BX Velocity and Vision stents and adjacent vectors were redirected in a more gradual manner since stent linkages are primarily arranged with the direction of flow. Interestingly, the Integrity stent, with its design arranged in a slightly pitched pattern along its length, also seems to impart a modest rotational component to velocity vectors as they proceed through the stented region that is associated with a slightly higher velocity than the Driver stent within intrastrut regions.

Mean exposure time results from the 2.25 mm diameter vessels are provided in Fig. 5. While the results are qualitative, the proximity and number of longitudinal or circumferential struts clearly impacts the MET. Struts in closer proximity have larger intrastrut

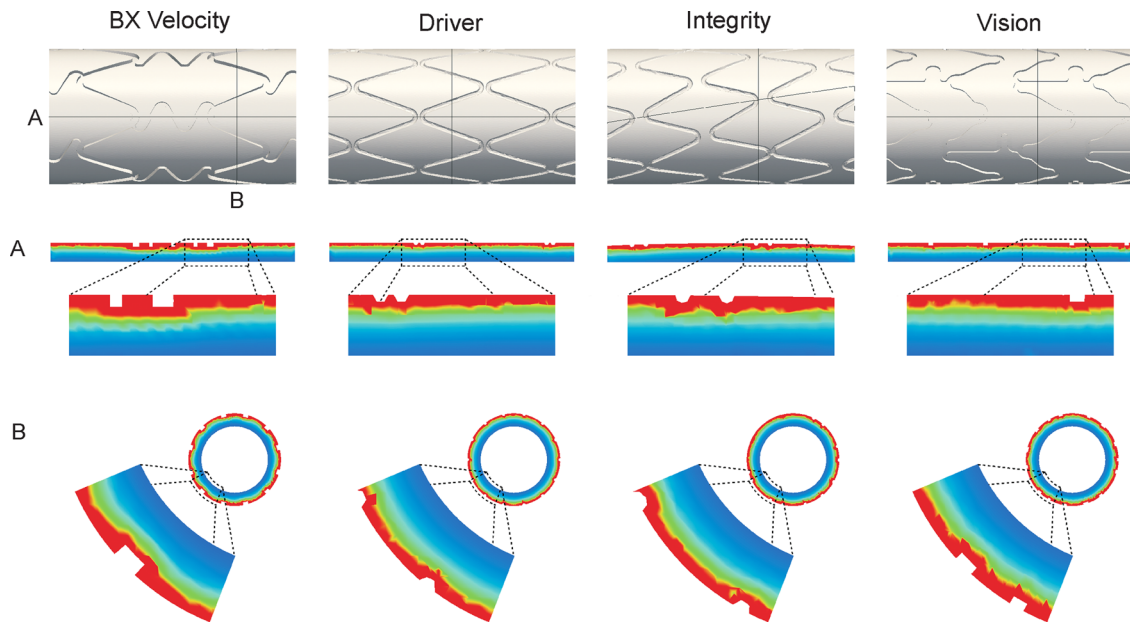


**Fig. 5** Mean exposure time (MET: range 0 to 0.45 s/cm) providing an indication of the average duration particles reside within various regions of each 2.25 mm diameter vessel. The portion of vessels shown (top) are from the middle of the stented region. (A) Longitudinal, and (B) generally circumferential slices are provided to qualitatively analyze the impact of strut thickness, proximity, and profile on the MET.

MET values, eg. Vision in Fig. 5(b) versus Integrity in Fig. 5(b). Strut thickness and profile also impact MET as thicker rectangular linkages increase the MET adjacent to struts (see Fig. 5; the BX Velocity and Vision stents) as compared to thinner struts having a circular profile (see Fig. 5; the Driver and Integrity stents). The BX Velocity has a stent thickness of 0.140 mm, the Vision has a stent thickness of 0.081 mm, and the Driver and Integrity have stent thicknesses of 0.090 mm. Thinner stent struts impart a positive benefit in terms of the WSS.

Figures 6 and 7 reveal the distributions of normalized TAWSS for all 3.00 and 2.25 mm diameter stents, respectively. The highest values of normalized TAWSS occur in the proximal and distal unstented regions and atop stent struts protruding into the flow domain, regardless of stent type. Lower normalized TAWSS values

occur adjacent to stent struts and are lowest downstream of struts oriented perpendicular to the primary direction of blood flow or in close proximity, such as the connector elements of the BX Velocity and Vision stents, along with the nonwelded crowns of the Driver and Integrity stents. The percentage of the vessel wall exposed to low normalized TAWSS (0.4) was also determined to more clearly reveal differences between the stents modeled in the current investigation (see Table 3). The BX Velocity stent had the greatest percentage of the vessel wall exposed to potentially deleterious distributions of TAWSS followed by the Vision, Integrity, and Driver stents. This order of TAWSS severity was the same for 2.25 and 3.00 mm diameter vessels. The BX Velocity stent had the thickest struts of the stents modeled, while Medtronic stents had the thinnest (70 versus 32  $\mu\text{m}$ , respectively). A slightly larger area of the vessel wall was exposed to low normalized TAWSS for the Integrity as compared to the Driver stents, regardless of size. Although strut thickness was the same for both stents, the stent to lumen area ratios for each size were slightly greater for the Integrity stents. The strut thickness was also comparable for the Vision and Integrity stents (41 versus 44  $\mu\text{m}$ , respectively; see Table 2). Although the Vision stents had a lower stent:lumen ratio than the Integrity stents within a given diameter (e.g., 0.18 versus 0.21 for 2.25 mm diameter vessels; see Table 2), the angle that their struts intersected with the primary flow domain was approximately double (e.g., 75–84 deg versus 42 deg; see Table 2) and, together with their connector elements, was likely the differentiating factor contributing to the higher percentage of the adverse TAWSS for the Vision stent. These findings suggest that strut thickness is an important determinant of the percentage of the vessel wall exposed to low normalized TAWSS. When the strut thickness and stent:lumen ratio are similar, the orientation of struts relative to the primary direction of blood flow can be a determining factor in the amount of the vessel exposed to the potentially deleterious values of TAWSS.

The percentage of vessels exposed to low normalized TAWSS was modestly increased for 3.00 mm as compared to the 2.25 mm diameter vessels for the Integrity (0.5%) and Driver (1.7%) stents. Conversely, this percentage decreased for 3.00 mm as compared with the 2.25 mm diameter vessels containing the Vision (2.4%) and BX Velocity (3.1%) stents. These findings can be explained

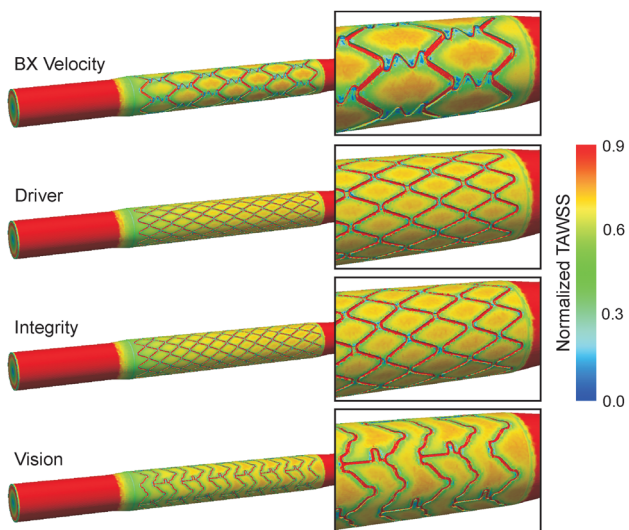


**Fig. 6** Time-averaged wall shear stress (TAWSS) normalized by the average wall shear stress in the proximal portion of each 3.0 mm diameter vessel

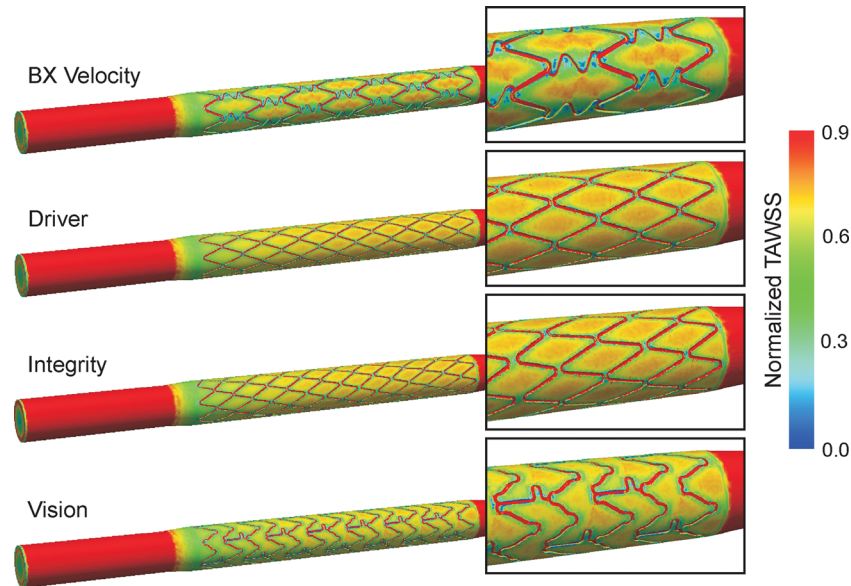


**Fig. 7 Time-averaged wall shear stress (TAWSS) normalized by the average wall shear stress in the proximal portion of each 2.25 mm diameter vessel**

**Table 3 Percentage of the vessel wall exposed to adverse TAWSS**

Stent name	Stent diameter (mm)	Total area (mm <sup>2</sup> )	Lumen area (mm <sup>2</sup> ) exposed to normalized WSS <0.4	Area exposed to low normalized WSS (%)
Integrity	2.25	140.0	8.34	5.95
	2.75	171.1	8.62	5.04
	2.75 (undersized vessel)	171.1	10.6	6.20
	3.00	186.6	12.0	6.42
Driver	2.25	140.0	6.57	4.69
	3.00	186.6	11.5	6.16
BX Velocity	2.25	140.0	24.4	17.4
	3.00	186.6	26.8	14.4
Vision	2.25	140.0	13.5	9.61
	3.00	186.6	13.4	7.18

by the stent:lumen area ratios in Table 2 and underscore one of the main findings of the current investigation. Within a stent type, the number of struts is a larger determinant of low TAWSS than the angle of intersection. In other words, the current results suggest that more favorable blood flow patterns may be achieved for a given stent design by limiting the number of linkages to those which provide adequate scaffolding.

Histograms of binned WSS values within intrastrut regions normalized to the respective intrastrut area of each stent studied are provided in Fig. 8. Data was obtained from equivalent intrastrut regions of the proximal, middle, and distal portions of the stents and for the two diameters studied. The histograms reveal several findings consistent with previous studies and also agree with intuition regarding blood flow through stents. The BX Velocity stents, having the thickest struts of those studied, along with the Vision stents with struts that have a large angle of intersection relative to the primary direction of fluid flow, cause more of the intrastrut area to be exposed to low normalized TAWSS (e.g. around 0.4–0.5), therefore resulting in a reduced peak at higher normalized TAWSS values as compared to the Driver and Integrity stents. Near-wall velocity patterns within the proximal, distal, and middle portions of stents provided in Fig. 9 suggest that the BX Velocity stent, with its pronounced sinusoidal connector elements that induce low velocity, act to restrict the intrastrut area, thereby increasing velocity in the center of the intrastrut regions and lead-

ing to associated higher values of TAWSS. This finding is also supported in Fig. 8. Although less of the normalized intrastrut area for any given location is exposed to elevated normalized TAWSS, the values of normalized TAWSS extend higher than with other stents due to the elevated velocity within the center of intrastrut regions for the BX Velocity stent.

**Comparison Between Integrity and Driver.** Reconciling the histogram data shown in Fig. 8 with the velocity and TAWSS patterns facilitates the comparison of the Driver and Integrity stents with confidence. Figure 8 demonstrates that the differences in the histograms between these stents are due to entrance effects likely induced by the helical winding process used to create Integrity stents. This process causes a modest geometric difference relative to Driver stents in the proximal region. As demonstrated in Fig. 4, these differences are essentially negligible beyond 8–10 mm of the stent as flow patterns assume their more developed profiles. Previous research suggests the slight helical nature of the Integrity stent likely allows flow within the stent to reach its developed profile a shorter distance from the proximal edge [24]. After flow patterns become developed, differences within the intrastrut regions between the Driver and Integrity stents are due to the proximity of adjacent stents, as shown in the instantaneous WSS plots of Fig. 9.

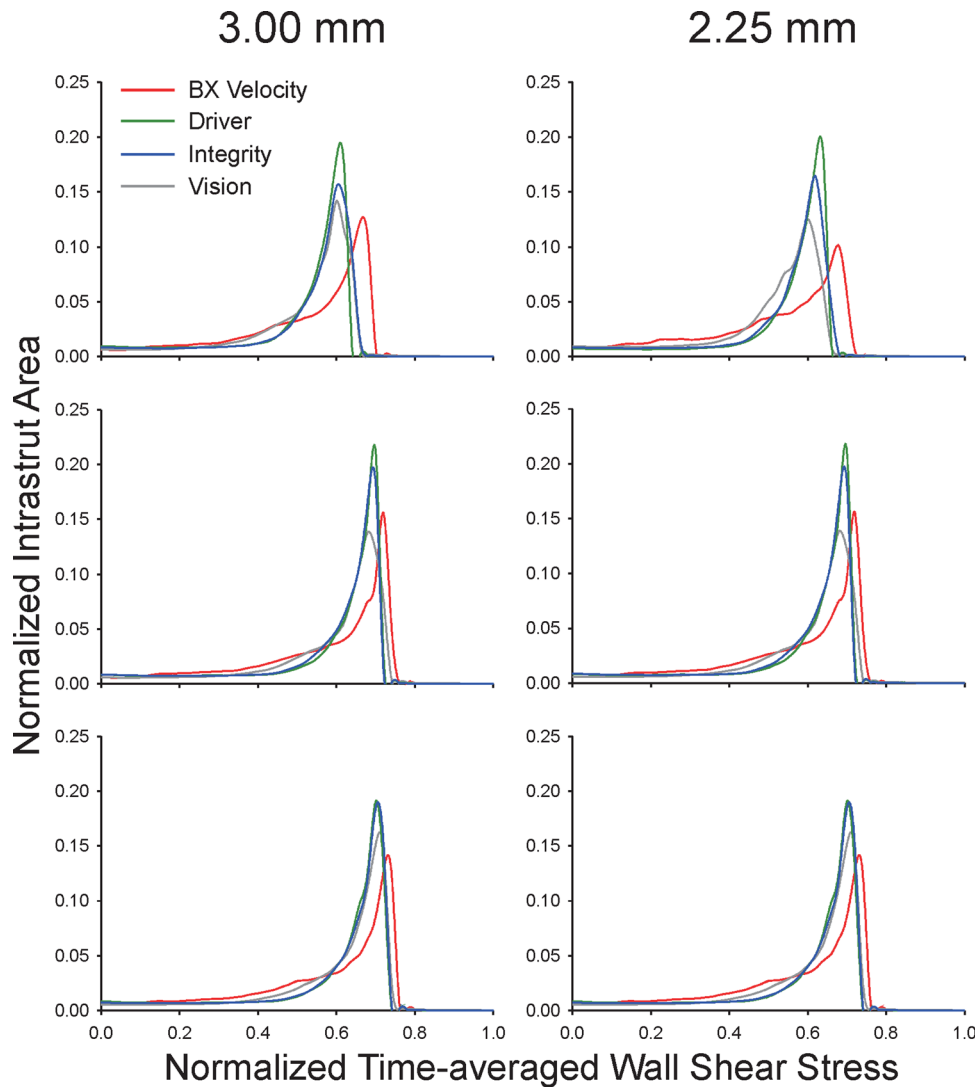


**Fig. 8** Histograms of the TAWSS within proximal (top), center (middle), and distal (bottom) intrastrut areas of each stent. It is desirable for histogram curves to have a large amount of their intrastrut area exposed to greater normalized time-averaged wall shear stress.

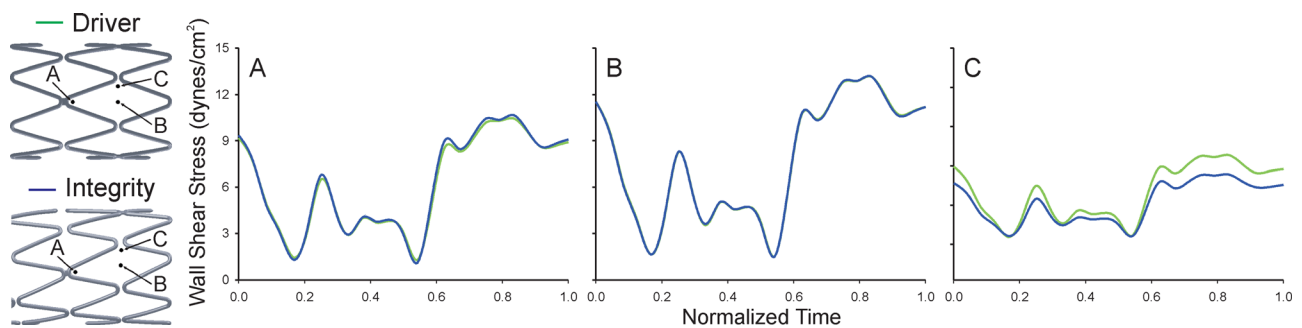


**Fig. 9** Instantaneous distributions of wall shear stress at three locations within intrastrut regions of Driver and Integrity stents. Tracings between the stents are indistinguishable at locations 'A' and 'B,' but slight differences in the relative proximity of struts at location 'C' causes modest differences in instantaneous values.

**Comparison Between Integrity Stents With Different Crown Configurations.** Results were also obtained for versions of 2.75 mm diameter Integrity stents with 7.5 or 9.5 crowns to quantify differences in the indices of interest from the best- and worst-case alignment of struts, with respect to the primary flow direction, as compared to the 2.25 or 3.00 mm diameter vessels for each crown configuration, respectively. Spatial distributions of

the TAWSS are shown in Fig. 10 and the amount of the vessel wall exposed to normalized TAWSS values less than 0.4 is depicted in Table 3. Modest differences were observed between vessels and, again, highlight the balance between stent:lumen area ratios and the angle of linkages relative to the primary direction of blood flow. Within the 7.5 crown configuration, the 2.25 mm simulation with a stent:lumen area ratio of 0.21 and an angle of

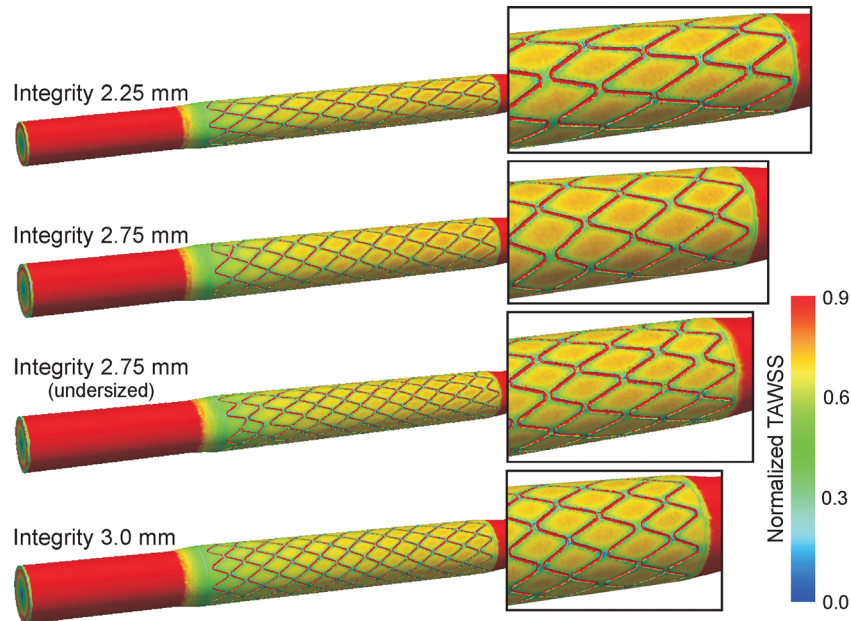


**Fig. 10 Time-averaged wall shear stress (TAWSS) normalized by the average wall shear stress in the proximal portion of the 2.25, 2.75, and 3.00 mm vessels containing Integrity stents with 7.5 crowns (2.25 and 2.75 mm) or 9.5 crowns (2.75 undersized vessel and 3.00 mm)**

42 deg relative to the flow direction had a slightly greater percentage of its surface exposed to low normalized TAWSS as compared to the 2.75 mm diameter vessel with a stent:lumen area ratio of 0.17 and an angle of 58 deg relative to the flow direction. Conversely, within the 9.5 crown configuration, the 2.75 mm simulation with a stent:lumen area ratio of 0.23 and an angle of 49 deg relative to the flow direction had a modestly lower percent of its surface exposed to low normalized TAWSS as compared to the 3.00 mm diameter vessel with a stent:lumen area ratio of 0.21 and an angle of 56 deg relative to the flow direction. Despite differences in the number of crowns, the 2.25 mm and 3.00 mm diameter vessels had the same stent:lumen area ratio, however, the 3.00 mm diameter vessel had a greater angle of struts relative to the flow direction and, hence, a greater percentage of the vessel wall exposed to potentially deleterious TAWSS. However, it is important to note that the maximum difference between the normalized TAWSS results shown from the collection of Integrity simulations is <1.5%, which is less than the difference between the 2.25 mm and 3.00 mm diameter vessels for the other three stent designs.

## Discussion

The current investigation tested the hypothesis that the slight modification in fabrication methods from the Driver stent to the Integrity stent results in nearly equivalent distributions of the WSS and flow stagnation patterns between the two stents and these differences are considerably less than between other commercially available bare metal stents when evaluated by CFD modeling. There were several key findings from the current investigation:

- Near-wall vectors indicate that the velocity is lowest surrounding stent struts and pronounced for stent designs where the angle of intersection between struts and the primary blood flow direction is greatest and connector elements deviate from the longitudinal direction.
- The intrastrut regions of the Driver and Integrity stents were exposed to favorable high near-wall velocities and the Integrity stent, with its design arranged in a slightly pitched/helical

pattern along its length, imparted a modest rotational component to these vectors, the potential advantages of which could be studied further in follow-up studies.

- The thickness, profile, proximity, and number of longitudinal or circumferential struts impacted the MET since struts that are closer together, thicker, and rectangular in profile increased the MET within the stented region.
- The BX Velocity stents had the greatest percentage of the vessel wall exposed to potentially deleterious distributions of TAWSS followed by the Vision, Integrity, and Driver stents. This order of severity was the same for the 2.25 and 3.00 mm diameter vessels.
- Strut thickness had the greatest impact on adverse distributions of the WSS. When this attribute was similar among designs, the stent:lumen area ratio, the angle of struts relative to the primary direction of blood flow, and the arrangement of connector elements were also predictive of adverse distributions of the WSS.
- Within a given stent type, the stent:lumen area ratio was a larger determinant of potentially adverse WSS than the angle of intersection, suggesting that more favorable blood flow patterns may be achieved for a stent design by limiting the number of linkages to those which provide adequate scaffolding.

These results confirm and extend previous findings in this area. For example, the lowest values of WSS were localized to the proximal and distal transition regions and adjacent to stent struts. Design attributes including strut thickness, proximity, angle relative to the primary flow direction, and the stent:lumen area ratio were generally predictive of potentially adverse distributions of the WSS, as demonstrated in prior studies [9,23,25]. To our knowledge, this is the first investigation that maintained detailed geometric specifications provided or extracted from manufacturer literature. In contrast, previous studies frequently approximated the geometric features of the stents including strut spacing and often employed a single thickness when comparing stents [26]. The current approach provided a slightly less controlled study having more variables to interpret, but also revealed what appears

to be a delicate balance between the flow disrupting design attributes of the strut intersection angle relative to the primary flow direction and the stent:lumen area ratio.

Pant et al. used axisymmetric models of five commercially available stents (ART, BX Velocity, NIR, Multilink Zeta, and Biomatrix) positioned in idealized cylinders using a 1:1 stent-to-artery implantation ratio [26]. The authors calculated indices, including the WSS, throughout the cardiac cycle, however, the TAWSS was not explicitly determined. A related study previously demonstrated that instantaneous WSS distributions corresponding to a time point near the mean flow rate for a simulation offers a reasonable estimate of the TAWSS [16]. If this logic is applied to the study by Pant et al., their results suggest that the ART slotted-tube design is most favorable from a flow perspective, followed by the BX Velocity, Biomatrix, NIR, and Multilink Zeta designs. However, stent:lumen area ratios were drastically different between designs and the absence of proximal and distal stent-to-artery transition regions also likely impacted these results.

The current results should be interpreted within the constraint of several potential limitations. A rigid wall assumption was employed for all simulations since stent implantation has been shown to decrease the arterial compliance to zero [14]. The inclusion of deformable walls in the proximal and distal portions of the CFD models would likely decrease the TAWSS, but in a similar manner for all stents modeled. To our knowledge, the BX Velocity stent is not available in an 18 mm version, as created for the current investigation. This adaptation was made to facilitate the direct comparison between stents and flow patterns with the stented region may be modestly influenced by the accompanying changes in parameters shown in Table 2 if the next nearest stent length (16 mm) had been used.

The stents studied in the current investigation were not implanted into a realistic environment and, therefore, do not contain local geometric attributes that could further influence local blood flow alterations for the indices reported. The work presented here elucidates differences purely due to stent design for the simple case of blood flow in a cylinder using the geometric properties of four balloon-expandable coronary stents. Nonetheless, the results are still impacting and applicable when appreciated within the context of several recent reports. While the specific weld locations for the Driver versus the Integrity stent may have an impact on post implantation morphology, the position of struts relative to one another and the resulting local blood flow patterns, a recent paper by Ormiston and colleagues [27] underscored how these stents, each having two weld locations joining sequential longitudinal repeating units, had a similar appearance after compression sufficient to cause 5 mm in shortening. The local deformation of strut linkages from this test were greater for the Vision and BX Velocity stents, suggesting that the differences between the Driver and Integrity relative to the Vision and BX Velocity stents may actually have been more pronounced had the current investigation been conducted in a realistic vessel. An extension of another recent computational study [28], conducted in a 135 deg bend with calcification and plaque at proximal and distal locations subjected to postdeployment by 10%, revealed nearly equivalent straightening, luminal volume, strut apposition, and induced vessel stress for the Driver and Integrity stents. Several previous studies conducted by our lab and others also have shown that for balloon-expandable stents, adverse local blood flow patterns induced by the geometry of an implanted stent can be mitigated or further accentuated by local vessel features, such as those influencing the curvature, apposition, and material properties of the vessel or plaque influencing prolapse. Hence, the current study was first conducted with a straight tube to delineate the differences in distributions of the WSS often masked by features of the flow domain that begin to present when using vessels with features such as curvature.

Several additional indices could have been used to characterize stent performance, including WSS gradients, WSS angle gradients, and peak WSS. Wall shear stress gradients have previously

been applied to idealized CFD models of stents [16]; while peak WSS values above some threshold can be associated with platelet activation, they are often reported to be of value for studies involving aneurysms and some reports have suggested that some vessels may remodel to peak, not mean, WSS [29]. While WSS gradient indices are useful for CFD studies conducted in idealized vessels, they have been omitted since they are more difficult to interpret when results are obtained from realistic subject-specific CFD simulations where small local geometric heterogeneities can mask the influence of stent attributes. Regardless of the approach used to interpret CFD results, it is important to note that the true contributions of each index will remain speculative until more detailed mechanotransduction studies are conducted to link each of these indices to the mechanisms of NH, either using specialized flow chambers seeded with confluent cell layers *in vitro* or coupled image-based CFD studies correlating WSS indices with local quantification by histology or OCT. The current results are nonetheless interesting since Verva Medical, a UK maker of stents, claims its BioMimics 3D stent, employing a helical geometry, promotes swirling of blood through stents that has been shown to reduce NH in preclinical studies [24].

In conclusion, the Driver and Integrity stents both limit their number of linkages to those which provide adequate scaffolding while also maintaining similar strut thickness and stent:lumen ratios. The Integrity stent also imparts a modest helical component previously shown to reduce NH *in vivo*. Collectively, these findings indicate the modest differences in the fabrication approach between the Driver and Integrity stents are not hemodynamically substantial, particularly relative to potentially adverse flow conditions introduced by the other stents modeled. This data was used in conjunction with associated regulatory filings and submitted to the FDA as part of the documents facilitating recent regulatory approval of the Integrity stent and the Integrity Shonin in Japan and the Resolute Integrity drug-eluting stent in the United States.

## References

- [1] Moses, J. W., Leon, M. B., Popma, J. J., Fitzgerald, P. J., Holmes, D. R., O'Shaughnessy, C., Caputo, R. P., Kereiakes, D. J., Williams, D. O., Teirstein, P. S., Jaeger, J. L., and Kuntz, R. E., 2003, "Sirolimus-Eluting Stents Versus Standard Stents in Patients With Stenosis in a Native Coronary Artery," *N. Engl. J. Med.*, **349**(14), pp. 1315–1323.
- [2] Gilbert, J., Raboud, J., and Zinman, B., 2004, "Meta-Analysis of the Effect of Diabetes on Restenosis Rates Among Patients Receiving Coronary Angioplasty Stenting," *Diabetes Care*, **27**(4), pp. 990–994.
- [3] Corbett, S. C., Ajdari, A., Coskun, A. U., and N-Hashemi, H., 2010, "In Vitro and Computational Thrombosis on Artificial Surfaces With Shear Stress," *Artif. Organs*, **34**(7), pp. 561–569.
- [4] Briguori, C., Sarais, C., Pagnotta, P., Liistro, F., Montorfano, M., Chieffo, A., Sgura, F., Corvaja, N., Albiero, R., Stankovic, G., Toutoutzas, C., Bonizzoni, E., Di Mario, C., and Colombo, A., 2002, "In-Stent Restenosis in Small Coronary Arteries: Impact of Strut Thickness," *J. Am. Coll. Cardiol.*, **40**(3), pp. 403–409.
- [5] Garasic, J. M., Edelman, E. R., Squire, J. C., Seifert, P., Williams, M. S., and Rogers, C., 2000, "Stent and Artery Geometry Determine Intimal Thickening Independent of Arterial Injury," *Circulation*, **101**(7), pp. 812–818.
- [6] Kastrati, A., Mehilli, J., Dirschinger, J., Dotzer, F., Schuhlen, H., Neumann, F. J., Fleckenstein, M., Pfafferott, C., Seyfarth, M., and Schomig, A., 2001, "Intracoronary Stenting and Angiographic Results: Strut Thickness Effect on Restenosis Outcome (Isar-Stereo) Trial," *Circulation*, **103**(23), pp. 2816–2821.
- [7] Gundert, T. J., Marsden, A. L., Yang, W., and LaDisa, J. F., Jr., 2012, "Optimization of Cardiovascular Stent Design Using Computational Fluid Dynamics," *ASME J. Biomech. Eng.*, **134**(1), p. 011002.
- [8] Gundert, T. J., Marsden, A. L., Yang, W., Marks, D. S., and LaDisa, J. F., Jr., 2012, "Identification of Hemodynamically Optimal Coronary Stent Designs Based on Vessel Diameter," *IEEE Trans. Biomed. Eng.*, **59**(7), pp. 1992–2002.
- [9] LaDisa, J. F. Jr., Olson, L. E., Guler, I., Hettrick, D. A., Audi, S. H., Kersten, J. R., Wartier, D. C., and Pagel, P. S., 2004, "Stent Design Properties and Deployment Ratio Influence Indexes of Wall Shear Stress: A Three-Dimensional Computational Fluid Dynamics Investigation Within a Normal Artery," *J. Appl. Physiol.*, **97**(1), pp. 424–430.
- [10] Gundert, T. J., Shadden, S. C., Williams, A. R., Koo, B. K., Feinstein, J. A., and LaDisa, J. F., Jr., 2011, "A Rapid and Computationally Inexpensive Method to Virtually Implant Current and Next-Generation Stents Into Subject-Specific Computational Fluid Dynamics Models," *Ann. Biomed. Eng.*, **39**(5), pp. 1423–1437.

- [11] Tanigawa, J., Barlis, P., and Di Mario, C., 2007, "Intravascular Optical Coherence Tomography: Optimisation of Image Acquisition and Quantitative Assessment of Stent Strut Apposition," *EuroIntervention*, **3**(1), pp. 128–136.
- [12] Muller, J., Sahni, O., Li, X., Jansen, K. E., Shephard, M. S., and Taylor, C. A., 2005, "Anisotropic Adaptive Finite Element Method for Modelling Blood Flow," *Comput. Methods Biomech. Biomed. Eng.*, **8**(5), pp. 295–305.
- [13] Sahni, O., Muller, J., Jansen, K. E., Shephard, M. S., and Taylor, C. A., 2006, "Efficient Anisotropic Adaptive Discretization of the Cardiovascular System," *Comput. Methods Appl. Mech. Eng.*, **195**(41–43), pp. 5634–5655.
- [14] LaDisa, J. F., Jr., Hettrick, D. A., Olson, L. E., Guler, I., Gross, E. R., Kress, T. T., Kersten, J. R., Warltier, D. C., and Pagel, P. S., 2002, "Stent Implantation Alters Coronary Artery Hemodynamics and Wall Shear Stress During Maximal Vasodilation," *J. Appl. Physiol.*, **93**(6), pp. 1939–1946.
- [15] LaDisa, J. F., Jr., Guler, I., Olson, L. E., Hettrick, D. A., Kersten, J. R., Warltier, D. C., and Pagel, P. S., 2003, "Three-Dimensional Computational Fluid Dynamics Modeling of Alterations in Coronary Wall Shear Stress Produced by Stent Implantation," *Ann. Biomed. Eng.*, **31**(8), pp. 972–980.
- [16] LaDisa, J. F., Jr., Olson, L. E., Guler, I., Hettrick, D. A., Kersten, J. R., Warltier, D. C., and Pagel, P. S., 2005, "Circumferential Vascular Deformation After Stent Implantation Alters Wall Shear Stress Evaluated With Time-Dependent 3D Computational Fluid Dynamics Models," *J. Appl. Physiol.*, **98**(3), pp. 947–957.
- [17] Williams, A. R., Koo, B. K., Gundert, T. J., Fitzgerald, P. J., and LaDisa, J. F., Jr., 2010, "Local Hemodynamic Changes Caused by Main Branch Stent Implantation and Subsequent Virtual Side Branch Balloon Angioplasty in a Representative Coronary Bifurcation," *J. Appl. Physiol.*, **109**(2), pp. 532–540.
- [18] Ellwein, L. M., Otake, H., Gundert, T. J., Koo, B. K., Shinke, T., Honda, Y., Shite, J., and LaDisa, J. F., Jr., 2011, "Optical Coherence Tomography for Patient-Specific 3D Artery Reconstruction and Evaluation of Wall Shear Stress in a Left Circumflex Coronary Artery," *Cardiovasc. Eng. Technol.*, **2**(3), pp. 212–217.
- [19] Vignon-Clementel, I. E., Figueroa, C. A., Jansen, K. E., and Taylor, C. A., 2006, "Outflow Boundary Conditions for Three-Dimensional Finite Element Modeling of Blood Flow and Pressure in Arteries," *Comput. Methods Appl. Mech. Eng.*, **195**(29–32), pp. 3776–3796.
- [20] Tang, B., Cheng, C., Draney, M., Wilson, N., Tsao, P., Herfkens, R., and Taylor, C., 2006, "Abdominal Aortic Hemodynamics in Young Healthy Adults at Rest and During Lower Limb Exercise: Quantification Using Image-Based Computer Modeling," *Am. J. Physiol. Heart Circ. Physiol.*, **291**(2), pp. H668–H676.
- [21] Lonyai, A., Dubin, A. M., Feinstein, J. A., Taylor, C. A., and Shadden, S. C., 2010, "New Insights Into Pacemaker Lead-Induced Venous Occlusion: Simulation-Based Investigation of Alterations in Venous Biomechanics," *Cardiovasc. Eng.*, **10**(2), pp. 84–90.
- [22] Malek, A. M., Alper, S. L., and Izumo, S., 1999, "Hemodynamic Shear Stress and Its Role in Atherosclerosis," *JAMA, J. Am. Med. Assoc.*, **282**(21), pp. 2035–2042.
- [23] Murphy, J. B., and Boyle, F. J., 2010, "A Full-Range, Multi-Variable, CFD-Based Methodology to Identify Abnormal Near-Wall Hemodynamics in a Stented Coronary Artery," *Biorheology*, **47**(2), pp. 117–132.
- [24] Shinke, T., Robinson, K., Gilson, P., Burke, M. G., Cheshire, N. J., and Caro, C. G., 2007, "Abstract 6059: Novel Helical Stent Design Elicits Swirling Blood Flow Pattern and Inhibits Neointima Formation in Porcine Carotid Arteries," *Circulation* **118**(18S), 1054.
- [25] Duraiswamy, N., Schoepfoerster, R. T., and Moore, J. E., Jr., 2009, "Comparison of Near-Wall Hemodynamic Parameters in Stented Artery Models," *ASME J. Biomech. Eng.*, **131**(6), p. 061006.
- [26] Pant, S., Bressloff, N. W., Forrester, A. I., and Curzen, N., 2010, "The Influence of Strut-Connectors in Stented Vessels: A Comparison of Pulsatile Flow Through Five Coronary Stents," *Ann. Biomed. Eng.*, **38**(5), pp. 1893–1907.
- [27] Ormiston, J. A., Webber, B., and Webster, M. W., 2011, "Stent Longitudinal Integrity Bench Insights Into a Clinical Problem," *JACC Cardiovasc. Intervent.*, **4**(12), pp. 1310–1317.
- [28] Mortier, P., De Beule, M., Segers, P., Verdonck, P., and Verheghe, B., 2011, "Virtual Bench Testing of New Generation Coronary Stents," *EuroIntervention*, **7**(3), pp. 369–376.
- [29] Ene-Iordache, B., Mosconi, L., Antiga, L., Bruno, S., Anghileri, A., Remuzzi, G., and Remuzzi, A., 2003, "Radial Artery Remodeling in Response to Shear Stress Increase Within Arteriovenous Fistula for Hemodialysis Access," *Endothelium*, **10**(2), pp. 95–102.